Magnetomotive Displacement of the Tympanic Membrane using Magnetic Nanoparticles: Toward Enhancement of Sound Perception

Pin-Chieh Huang, Eric J. Chaney, Ryan L. Shelton, and Stephen A. Boppart, *Fellow, IEEE*

***Abstract*— *Objective:* A novel hearing-aid scheme using magnetomotive nanoparticles (MNPs) as transducers in the tympanic membrane (TM) is proposed, aiming to noninvasively and directly induce a modulated vibration on the TM. *Methods:* In this feasibility study, iron-oxide (Fe_3O_4) nanoparticles were applied on *ex vivo* rat TM tissues and allowed to diffuse over ~2 hr. Subsequently, magnetic force was exerted on the MNP-laden TM via a programmable electromagnetic solenoid to induce the magnetomotion. Optical coherence tomography (OCT), along with its phase-sensitive measurement capabilities, was utilized to visualize and quantify the nanometer-scale vibrations generated on the TM tissues. *Results:* The magnetomotive displacements induced on the TM were significantly greater than the baseline vibration of the TM without MNPs. In addition to a pure frequency tone, a chirped excitation and the corresponding spectroscopic response were also successfully generated and obtained. Finally, visualization of volumetric TM dynamics was achieved. *Conclusion:* This study demonstrates the effectiveness of magnetically inducing vibrations on TMs containing iron-oxide nanoparticles, manipulating the amplitude and the frequency of the induced TM motions, and the capability of assessing the magnetomotive dynamics via OCT. *Significance:* The results demonstrated here suggest the potential use of this noninvasive magnetomotive approach in future hearing aid applications. OCT can be utilized to investigate the magnetomotive dynamics of the TM, which may either enhance sound perception or magnetically induce the perception of sound without the need for acoustic speech signals.**

***Index Terms*—Magnetic nanoparticles, optical coherence tomography, magnetomotive, hearing aids, tympanic membrane**

I. Introduction

HEARING impairment has an overall prevalence of 48.1 million for individuals above 12 years old and is the third most prevalent chronic condition for older individuals in the United States [1, 2]. Normally, sound is transferred from the outer ear to the middle ear, where it vibrates the ear drum/tympanic membrane (TM). The auditory ossicles subsequently transduce the vibrations to the cochlea in the inner ear, where the acoustic waves are converted to neural signals by the hair cells within the cochlea (Fig. 1). The most prevalent type of impairment – sensorineural hearing loss (SNHL), most commonly associated with aging, is a result of damaged hair cells, decreased blood supply to the cochlea, and defects in neural elements such as the synapses between the spiral ganglion neurons and the hair cells in the cochlea [1, 3, 4]. There is currently no treatment for damaged neural elements, and hence, most SNHL is treated, although not cured, with conventional hearing aids that enhance sound perception by amplifying the amplitude of the sound [1]. However, traditional hearing aids are frequently dissatisfying due to their ineffectiveness in noisy or high-frequency environments, the presence of undesirable acoustic feedback, the occlusion effect, a lack of sound localization cues, and general discomfort [3, 5, 6]. Alternative treatments for mild to severe hearing impairment include middle ear implants, where a subcutaneously-implanted vibrating ossicular prosthesis converts sound to mechanical vibrations, which are then carried out by a magnet transducer that is often crimped to the incus to directly drive the ossicular chain [3, 7]. For conductive hearing loss, other mechanical hearing implants such as the bone-conduction devices (BCD) can be utilized as well. With BCD, acoustic vibrations can be transmitted from the implanted screws to the skull bone either directly or indirectly (through skin), so that the vibrations can reach the inner ear without being affected by the impaired outer or middle ear [8]. However, the invasive surgery to implant these devices naturally comes with risks, and is undesirable.

Different from conventional acoustic hearing devices and the ear implants, a non-invasive way of magnetically and directly vibrating the TM and the auditory ossicles without the stimulation of acoustic speech signals has been previously proposed and demonstrated. An "EarLens" device has been developed, which is composed of a solid transducer embedded in a cone-shaped, thin, silicone rubber platform that can be placed above the umbo area of the TM [6]. One type of EarLens

Manuscript received XXX, XXXX. This work was supported in part by the National Institutes of Health (R01 EB013723 and R01 CA213149).

P.-C. Huang is with the Biophotonics Imaging Laboratory, Beckman Institute for Advanced Science and Technology, and the Department of Bioengineering, University of Illinois at Urbana-Champaign, Urbana, IL 61801 USA (e-mail: phuang16@illinois.edu).

E. J. Chaney and R. L. Shelton are with the Biophotonics Imaging Laboratory and the Beckman Institute for Advanced Science and Technology, University of Illinois at Urbana-Champaign, Urbana, IL 61801 USA (e-mail: echaney@illinois.edu; rlshelt@illinois.edu).

*S. A. Boppart is with the Biophotonics Imaging Laboratory, Beckman Institute for Advanced Science and Technology, and the Departments of Electrical and Computer Engineering, Bioengineering, and Medicine, University of Illinois at Urbana-Champaign, Urbana, IL 61801 USA (correspondence e-mail: boppart@illinois.edu).

This article has been accepted for publication in a future issue of this journal, but has not been fully edited. Content may change prior to final publication. Citation information: DOI 10.1109/TBME.2018.2819649, IEEE Transactions on Biomedical Engineering

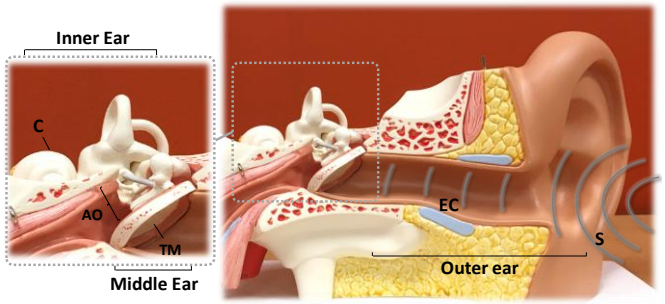

Fig. 1. Ear anatomy and the hearing principle. The sound waves (S) travel through the ear canal (EC) to the middle ear where they vibrate the ear drum/tympanic membrane (TM) and the auditory ossicles (AO). These vibrations reach the inner ear, where the hair cells inside the cochlea (C) convert the vibration to neural signals so that the brain can interpret sound.

transducer is a solid magnet, which could respond to and hence be controlled by a magnetic field generating device. Clinical experiments were conducted with a system composed of a magnetic EarLens transducer, a sound processor, and an ear-canal transceiver (with a coil and a microphone placed at the ear canal) [5]. By placing the transducer directly on the TM, a wider frequency range was produced as compared to conventional hearing aids. Note that with a direct-drive magnetic hearing implant, improved functional gain and word recognition have been reported for high-frequency SNHL patients in a preliminary study [9]. In the EarLens system, similar to the open-fit model utilized in many modern hearing aids, the microphone did not seal the ear canal like earmolds. This open-fit configuration may reduce the occlusion effect (especially at low frequencies), unwanted acoustic feedback, and improve one's perception of his/her own voice.

The EarLens platform has made the attachment of a magnet to the TM more tolerable and has inspired other solid-transducer-based hearing devices and investigations [5, 10, 11]. To use this platform, mineral oil was applied to keep the transducer and the TM in contact. However, two major improvements over this design are desired. First, sophisticated and delicate procedures are required to achieve an accurate placement and later removal of the transducer from the TM, with both procedures requiring professional assistance from a physician [10]. Additionally, each silicone-rubber-based platform needs to be customized for each wearer due to the individual variations of ear-canal anatomy [5, 10]. Second, the magnet transducer provides a non-negligible weight (mg-scale) on the TM, which could dampen the sound vibrations to some extent and may affect the perceived sound quality [5, 10].

In this report, we propose and demonstrate a novel hearing-assistance scheme that uses superparamagnetic magnetic nanoparticles (MNPs) applied to and diffused into the TM. Similar to the EarLens system, an external alternating magnetic field (AMF) exerts a magnetic force, and hence, directly induces movement of the TM. The advantages of using MNPs as TM transducers are five-fold. First, superparamagnetic MNPs have high magnetic susceptibilities as compared to that of typical biological tissues, and they can only be magnetized upon application of an external magnetic field. Therefore, remote modulation of the MNP-laden tissues with high selectivity and sensitivity is enabled [12]. Second, other than going through the difficulty of customizing, placing, and removing the solid transducer on/off of the TM, the MNPs are envisioned to be applied as a form of an "ear drop" – which only requires a few drops of MNP solution to diffuse into the TM over time. Much like the standard treatment of sudden SNHL, where a large dose of drug was injected into the middle ear cavity and allowed to diffuse into the inner ear passively [13], here, the applied MNPs were expected to passively diffuse into the TM. In a living animal, MNP uptake by fluid endocytosis would also be expected [14]. If further guidance of MNP diffusion is desired, additional magnetic field assistance, such as has been proposed for drug delivery applications, can be implemented [14-16]. Third, MNPs carry negligible mass, and hence can potentially reduce the dampening effect of the TM. Fourth, unlike the current solution that only allows for a single load point, MNP drops can potentially provide a more uniform loading across the TM and hence result in a more natural TM vibration response. Finally, it is well known that the iron-oxide MNPs can degrade into oxygen and iron and be physiologically cleared from the systematic circulation by macrophages [17]. This clearance process may potentially occur after the administrated MNPs are released in the human body after exocytosis or apoptosis, travel through the Eustachian tube and the throat, swallowed, and enter the human body [14]. The MNPs can be further functionalized to enhance their biocompatibility and biodegradability as well [18]. Note that as the iron-oxide MNPs degrade or are shed and lost over time, repetitive administration of the MNP drops to the TM may be necessary.

A few early publications have investigated techniques for loading TMs with MNPs, and utilized laser Doppler interferometry (LDI) to measure the magnetically-induced motion of MNP-laden TMs in guinea pigs [14, 19]. These studies carefully and substantially investigated the internalization approach and the biocompatibility of the MNPs in biological systems from a physiological perspective. However, the magnetically-induced TM motions, characterized via single-point LDI, has been limited to only surface motion measurements at one location under two specific magnetic excitation frequencies. Other than LDI [20, 21], holography [22, 23] has also been reported as another optical imaging tool for estimating the local displacement or to visualize the dynamics of the moving TM, which, again, can only measure the motion of the TM surface.

Optical coherence tomography (OCT) is a non-invasive, depth-resolved imaging technique analogous to ultrasound imaging and has been widely applied for biomedical imaging applications [24]. The micrometer resolution of OCT has equipped it with the capability of imaging fine details of the retina [25, 26], breast tissue [27, 28], skin [29, 30], and the ear [31-33], just to name a few. Based on the cross-sectional, depth-resolved structure revealed by OCT or low-coherence interferometry (LCI), our group has previously demonstrated the feasibility of detecting bacterial biofilms beneath the TM and in the middle ear space [31-34] as well as the temporal response of the TM to a pneumatic pressure stimulus [35], demonstrating the advantages of using OCT for ear imaging.

Relying on the phase-resolved information extracted from the complex OCT data, the motion of the imaged tissue can be revealed with a sub-nanometer displacement sensitivity. By taking advantage of this phase-sensitive measurement capability with OCT, a number of researchers have successfully visualized the depth-resolved motion of the TM in response to sound stimulation [36-39]. Here, we aimed to use phase-sensitive OCT to evaluate the TM dynamics after electromagnetic stimulation, rather than after sound (acoustic wave) stimulation. The combined use of MNPs as perturbative agents and phase-sensitive OCT as a detection tool for the induced "magnetomotion" has been previously developed and reported as magnetomotive OCT (MM-OCT) [40-45], which will be discussed in more detail in Section II.

This initial study aims to evaluate the feasibility of using MNPs as "ear drop" TM transducers, with the capability of these to remotely respond to the external application of a magnetic field produced by an electromagnetic coil, and to directly induce vibrations on the TM without any ambient sound stimulation from the outer ear. Similar to the processing in MM-OCT, phase information was extracted from OCT images. However, while MM-OCT typically detected the presence of MNPs and provided the magnetomotion amplitude in a relative manner (in dB), this study further quantified the absolute values (in nm) of the induced displacement of the TM. Spectroscopic responses of the magnetomotive displacements were also examined, while cross-sectional visualization of the induced vibrations was provided by MM-OCT for *ex vivo* rat TMs.

II. Magnetomotion and Phase-Sensitive OCT

Magnetomotive OCT (MM-OCT) is a functional imaging modality proposed in the 2000s by our group, where MNPs that have been delivered to the tissues are actuated by an external magnetic field gradient and subsequently transduce vibrations to the MNP-laden samples to provide sub-resolution dynamic imaging contrast in OCT images [41, 45]. The MM configuration is exploited in this study to produce a controllable magnetic force and hence generate modulated displacements (termed "magnetomotion") on the MNP-laden TM tissues, which can be visualized by phase-sensitive OCT.

The magnetic force ($\vec{F}_{MNP}$) exerted on a single spherical MNP can be described as $\overrightarrow{F_{MNP}} = \frac{V_{MNP}\Delta\chi}{\mu_0}\left(\vec{B}\cdot\nabla\right)\vec{B}$ [46]. Therefore, the two key requirements for producing a sufficiently strong magnetic force include having (1) a noticeable magnetic field gradient (so that $\left(\vec{B}\cdot\nabla\right)\vec{B}\neq 0$) and (2) a large difference between the magnetic susceptibility of the MNP and that of the surrounding medium $\Delta\chi$ (as the permeability constant, μ_0, and the volume of the MNP, V_{MNP}, are fixed). In practice, a magnetic field gradient can be generated in the MNP-laden tissue by placing an external magnetic solenoid, which produces an AMF, nearby. A high $\Delta\chi$ can be readily achieved by using superparamagnetic MNPs as their magnetic susceptibilities are at least five orders of magnitude greater than that of the surrounding tissue [42]. To produce a sinusoidal oscillating magnetic force (and hence the induced magnetomotion), an alternating voltage (V) with a square root of sine pattern can be used to drive the magnetic solenoid as $\overrightarrow{F_{MNP}} \propto |\vec{B}|^2 \propto V^2$ at the low $|\vec{B}|$ regime [42].

The induced magnetomotion can be subsequently detected via phase-sensitive OCT, where the phase-resolved data can be obtained and the tissue displacement, $dz(dt)$, over a time interval, dt, can be revealed by the phase differences, $d\phi(dt)$ between adjacent A-scans (that are oversampled along transverse direction) via $d\phi(dt) = \frac{4\pi n}{\lambda_0} dz(dt)$ [47], assuming both the tissue refractive index, n, and the center wavelength of the light source, λ_0, remain unchanged during imaging.

MM-OCT is often applied to detect the presence of the dynamically modulated signal and identify the MNP-labeled regions in biological tissues [40, 43, 44]. However, this report emphasizes the quantification of the magnetomotive displacement induced on the MNP-laden TM tissues. Although MM-OCT has been widely explored in the field of biomedical research, this is the first time that magnetomotion is generated on TM tissues and visually assessed via phase-sensitive OCT.

III. Methods

A. Tissue Preparation and Iron-Oxide Staining

All animal care and handling procedures in this study were conducted under a protocol approved by the Institutional Animal Care and Use Committee (IACUC) at the University of

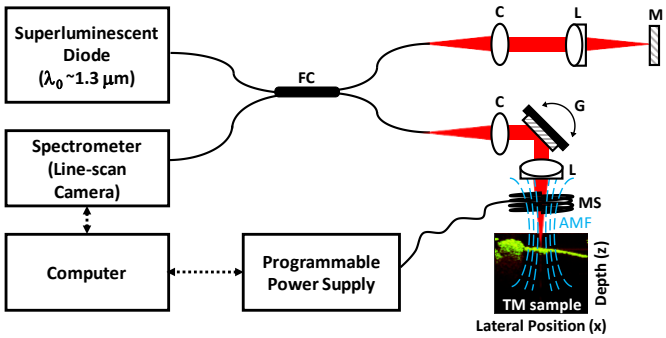

Fig. 2. Schematic of the magnetomotive OCT (MM-OCT) system. A superluminescent diode (center wavelength ~1310 nm) produces near-infrared light that is sent through a single-mode fiber, where a 2×2 fiber coupler (FC) splits the light into two beams. One beam travels to the reference arm, which is composed of a fixed mirror (M); the other beam passes through the sample arm to the TM tissue sample. The backscattered light from both the sample and reference arms interfere, and the resulting interference pattern is detected by the spectrometer. A magnetic solenoid (MS) is placed in the sample arm, where the light beam passes through the bore of the MS to the tissue sample. The alternating magnetic field (AMF) is generated by applying different driving voltage waveforms to the MS with a programmable power supply. Other optical components in the system include the collimator (C), the achromatic lens (L), and the galvanometer scanner (G).

Illinois at Urbana-Champaign. In this study, a total of 7 female F344/NHsd rats (age 6–10 weeks) (Envigo) were used. The TMs were obtained by harvesting the tissues immediately after euthanasia by CO_2 inhalation. Each rat TM specimen was isolated from the body to allow for *ex vivo* imaging. The temporal bone was first removed from the skull and subsequently cut to expose the middle ear cavity. Similar to the specimens prepared in a previous study [48], in each specimen, the ear canal, tympanic annulus (which surrounds the TM), and the malleus were included. However, the incus was not part of the harvested tissue. Due to the inherent anatomical curvature of the ear canal, the outer ear was adequately trimmed to allow for better accessibility for the OCT imaging beam. After the dissection, the entire tissue (TM along with the surrounding tympanic annulus) was placed in a Petri dish. A small piece of tube-shaped wax (Surgident), sandwiched between the tympanic annulus and the Petri dish substrate, was used to mount the tissue specimen in place and prevent the TM from directly contacting the Petri dish substrate. The TM specimens were placed in ambient air.

Subsequently, 0.1 ml of the MNP solution (10 mg/ml or 5 mg/ml of iron oxide nanoparticles, Fe_3O_4, phosphate-buffered-saline-based) was applied to the TM tissue from the outer ear side using a 22-gauge syringe, applied in a manner that is analogous to ear drops. The non-coated Fe_3O_4 nanoparticles utilized here (#637106, Sigma-Aldrich) were characterized previously [42]. A 10 ml MNP solution with a fixed Fe_3O_4 concentration was first prepared in a centrifuge tube (#430055, Corning), which was subsequently dispersed by a vortex mixer (Vortex-Genie 2, Scientific Industries) until the MNP solution was visually mixed in the PBS. Immediately after the mixing, a 1-ml syringe (BD) was used to suction the amount of MNP solution needed from the center of the entire solution volume, where 0.1 ml of the solution was subsequently applied to the TM. Minimal clustering of the Fe_3O_4 nanoparticles was observed by the time the administration of the MNP drops was completed. For the control group, 0.1 ml of phosphate-buffered saline (PBS) was applied instead. The solution, MNP or PBS, was left in place for ~2 hr to allow for MNP diffusion into the TM, with a permanent magnet (magnetic stir bar, 77 mm × 13 mm) positioned at ~8 mm beneath the TM tissue (on the inner ear side) to potentially assist the diffusion of MNPs into the TM. To also investigate and visualize the dynamics of the TM, one TM sample was fully immersed in the MNP solution (10 mg/ml) for ~44 hr to ensure a thorough and uniform distribution of the MNPs. Note that this sample was excluded from the analyses presented in Sections IV.A.–IV.C.

Prussian blue histological staining of the TMs was performed after each experiment, which selectively stained the iron-oxide blue/purple. After OCT imaging, the TM tissue (surrounded by temporal bone) was immediately immersed in Formalin for at least 6 hr, and then immersed in decalcification solution (D0818, Sigma-Aldrich) for another 6–8 hr. Subsequently, the Formalin-fixed and decalcified tissues were embedded in paraffin, sectioned, and stained with the iron-oxide staining kit (HT20, Sigma-Aldrich). A rat spleen sample was used as a positive control to ensure the effectiveness of the staining because iron naturally accumulates in this organ and it is known to stain positive with Prussian blue [17].

B. Experimental Setup

A custom-built spectral-domain OCT (SD-OCT) system (Fig. 2) was utilized for imaging. The system specifications were detailed previously [49]. In brief, the OCT system contains a broadband superlumenicent diode light source (LS2000B, Thorlabs) with a center wavelength of 1310 nm and a bandwidth of 170 nm, which provides an axial and lateral resolution of ~6 μm and ~16 μm, respectively. The phase noise measured at 2 kHz is ~0.17 rad, which corresponds to a displacement sensitivity of ~18 nm (optical distance). In the spectrometer, a 1024-pixel InGaAs line-scan camera (SU-LDH2, Goodrich) was used. The reference arm consists of a static mirror. In the sample arm, an electromagnetic solenoid was placed between the TM tissue sample and the objective lens. The near-infrared light beam was allowed to reach the TM tissue through the bore (~2 mm) of the solenoid, which was encased in a hollow, cylindrical plastic container (diameter ~46 mm) where the spacing allowed for circulation of cooling water. The customized solenoid had an inner diameter of 6 mm and a height of 10 mm. Driven at 8 V (peak) via a programmable power supply, the current passing through the coil was approximately 2.6 A.

During the application of an AMF, a peak field strength of ~184 G was applied, and the sinusoidal driving waveform was operated at a frequency range across 50–500 Hz. The tissue samples were placed ~2 mm beneath the electromagnetic solenoid.

C. Determination of the Modulated Frequency Range

As a preliminary step of exploring the feasibility of inducing magnetomotion on rat TM and detecting the subtle displacement via phase-sensitive OCT, a low-frequency, pure

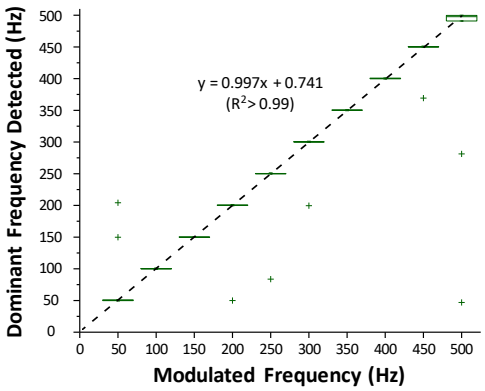

Fig. 3. Validation of the correlation between the modulated frequency applied (f_m) and the dominant frequency detected (f_d) from the 10 mg/ml MNP-laden TM tissues (N = 12–16 for each frequency value). The dashed line denotes the linear fit of the median f_d . For both (a) and (b), the "+" symbols shown beyond the whisker regions indicate the outliers (defined with an outlier coefficient of 3).

tone stimulation up to 500 Hz was given in this study. The low-frequency range was chosen for two main reasons. First, this initial study focused on visualization and quantification of the vibration of in-phase, pure tone TM motions, which could not be observed with higher modulated frequency (>1 kHz), where complex vibrational modes and multiple out-of-phase motions occur across the TM surface [20, 22, 23, 37, 48]. In addition, although the resonant frequency of the rat TM typically occurs at higher frequency [50], the disruption of the ossicular chain behind a TM specimen could result in a downshifting of its resonant frequency [20-22, 51].

The resonant frequencies were determined as the modulated frequencies that provide the maximum displacement induced on the TM. While the frequency responses of TMs often show multiple local displacement peaks at different frequency ranges [50], it should be clarified that the "resonant frequencies" stated in the rest of the paper refer to the resonant frequency at the low frequency range (≤ 500 Hz), in which local resonant peaks have been observed before [48].

D. Data Acquisition and Processing

A variety of excitation configurations, along with the corresponding data acquisition and processing approaches, have been applied to demonstrate different capabilities of the proposed magnetomotive hearing (MM-hearing) method.

1) Harmonic excitation

Magnetic force was first applied with a sinusoidal waveform to induce a harmonic oscillation on the TM tissues. The modulated frequencies were from 50 to 500 Hz, with a frequency interval of 50 Hz. B-mode scanning was performed with the modulated magnetic field being turned on ("field-on") and off ("field-off"). During data collection, 4,000 A-scans were obtained while scanning across a transverse range of ~2 mm so that spatial oversampling was achieved. The line scan rate was set to ~3 kHz to ensure that the sampling was sufficient and that the Nyquist criterion was met. In post-processing, phase differences between adjacent A-scans were obtained. Binary thresholding was conducted on the phase difference map based on the intensity levels (masking the area which has an intensity < 60% maximum intensity). Phase unwrapping was performed afterwards.

To isolate the magnetomotion modulated at a specific frequency, bandpass-filtering was applied to the unwrapped phase difference data in the Fourier domain. By taking the absolute value after the inverse Fourier transform, the corresponding displacement amplitude was therefore quantified. Subtracting the displacement of the "field-off" from that of the paired "field-on" datasets produced the magnetomotive displacement (termed "MM-displacement" throughout this paper) map, while the spatially averaged MM-displacements were utilized and analyzed statistically. Note that the MM-displacements were calculated by assuming a refractive index n = 1.4, which is the approximate value reported for human TMs [52].

The detected motions of the TM tissue truly originated from the induced magnetomotion instead of undesirable experimental motion artifacts caused by stage or table jittering as dominant displacement peaks can be observed from the transfer function. In addition, the dominant displacement frequencies detected (f_d) from the TM motion correlated well with the corresponding modulated frequencies (f_m) used for excitation in the MNP-laden TM tissues (shown in Fig. 3, the linear fit gives an almost one-to-one correspondence between f_d and f_m). Finally, the potential influence of the mechanical coupling from the magnetic coil vibration to the tissue is insignificant as negligible MM-OCT signals were detected on non-MNP-laden tissues under magnetic stimulation, demonstrated in our previous study [12]. Note that the transfer function was obtained by dividing the "field-on" over the "field-off" spectra in the Fourier domain with a regularization term implemented, where each spectrum was obtained by first averaging the thresholded phase difference map along depth and subsequently performing a Fourier transform along the transverse direction (the phase difference values were similar along depth, possibly due to the relatively small TM thickness and the fibrous components within the TM that are mechanically coupled to one another). Subsequently, f_d was determined as the frequency that gave the maximum peak amplitude in the transfer function.

2) Spectroscopic excitation

Other than a harmonic excitation, a chirped signal with frequencies swept through 10–500 Hz was also applied, while M-mode acquisition was performed. The line scan rate was selected to be ~2 kHz to meet Nyquist sampling criteria. The post-processing procedures for phase retrieval and spectral analysis were similar to those described earlier, however, with the use of M-mode data instead. Note that band-pass-filters were not implemented in this case. On the other hand, the temporal tissue displacement was utilized to produce a spectrogram, which illustrates the spectral component at each temporal instant via a short-term Fourier transform (STFT).

3) Dynamic motion visualization

Similar to the process reported previously [49], an AMF with a 460 Hz sinusoidal waveform was applied, synchronized to the galvanometer triggering, and the M-B mode data were acquired. M-scans were obtained across a transverse area of ~1.6 mm × 1.6 mm (60 × 60 data points), while at least 200 M-scans were acquired at each location with a line scan rate of ~92 kHz. Eventually, a volumetric dataset was obtained for each time point. Again, the modulated magnetomotion was extracted from the band-pass-filtered phase differences. Subsequently, dynamics of the magnetomotion were visualized by amplifying the phase by a factor of 50 and translating it into pixel-scale movements. By streaming each volumetric OCT data over time,

TABLE I
SAMPLE SIZE

Number of:	10 mg/ml MNP	5 mg/ml MNP	PBS (Control)
TMs	4	3	3
Locations	4	4	4
MM-displacements[a]	16	12	12

[a]Only the maximum MM-displacement measured (at the resonant frequency of the TM) was included in the statistical analysis.

This article has been accepted for publication in a future issue of this journal, but has not been fully edited. Content may change prior to final publication. Citation information: DOI 10.1109/TBME.2018.2819649, IEEE Transactions on Biomedical Engineering

a four-dimensional (4D) dataset was produced. Note that linear interpolation along the transverse directions were implemented, and hence each volumetric OCT data has a pixel dimension of 600 (x) × 600 (y) × 512 (z).

E. Statistical Analysis

To reduce the probability of false discoveries (false significant results) during multiple hypotheses testing, Bonferroni correction was performed after two-sample *t*-tests. Therefore, the *p*-values reported in this study refers to the adjusted *p*-value, obtained by n_t × unadjusted *p*-value, where n_t is the total number of tests performed [53]. All statistical analyses were carried out using Matlab (MathWorks). For each group (i.e. 10 mg/ml MNP, 5 mg/ml MNP, and control), the number of TM tissues involved, measurement locations, and the total sample sizes for MM-displacement analyses (Sec. IV. B.) are all documented in Table I.

IV. Results

A. MNP Diffusion and Iron-Oxide Staining

To validate the presence of the MNPs in the TM tissues, Prussian blue (iron-oxide) stained histologic tissue sections were imaged via a commercial microscope (Axiovert 200, Carl Zeiss). Representative images of the MNP-laden and control TM samples are shown in Fig. 4 (a), where the Prussian blue staining shows the presence of iron oxide MNPs. The iron oxide MNPs were located at the same focal plane as the TM tissue and could only be found in the MNP-laden samples. In addition, the MNPs appeared as dark blue-stained clusters in the microscopic images, similar to other microscopic images of Prussian-blue stained MNPs in tissue reported in literature [15]. Non-clustered MNPs were also observed at some locations (data not shown), however the clusters were more common and apparent, which could be attributed to the inevitable sloughing off of individual MNPs during the sectioning and staining processes. Note that due to the high magnification (100x) utilized, sharp contours from the tissue specimen could only be observed partially as slightly non-flat structure can easily fall outside of the tight focal plane.

Based on the Prussian blue staining outcome, the presence of the MNPs in the MNP-laden tissues was validated. Hypothetically, passive diffusion could result in a lower amount of MNPs being bound to the TM. However, future validation and understanding of the MNP distribution across the TM, as well as the investigation of the cellular uptake mechanisms (endocytotic or non-endocytotic pathways [14, 54]) of MNPs in *in vivo* TM via techniques that can avoid tissue sectioning artifacts such as micro-computed tomography (micro-CT) and high-field magnetic resonance imaging (high-field MRI) [55, 56], are desirable. In addition, further permeabilization of the TM can be implemented via chemical approaches [57] and the MNP uptake can be promoted by using biocompatible MNPs [58] for future *in vivo* studies.

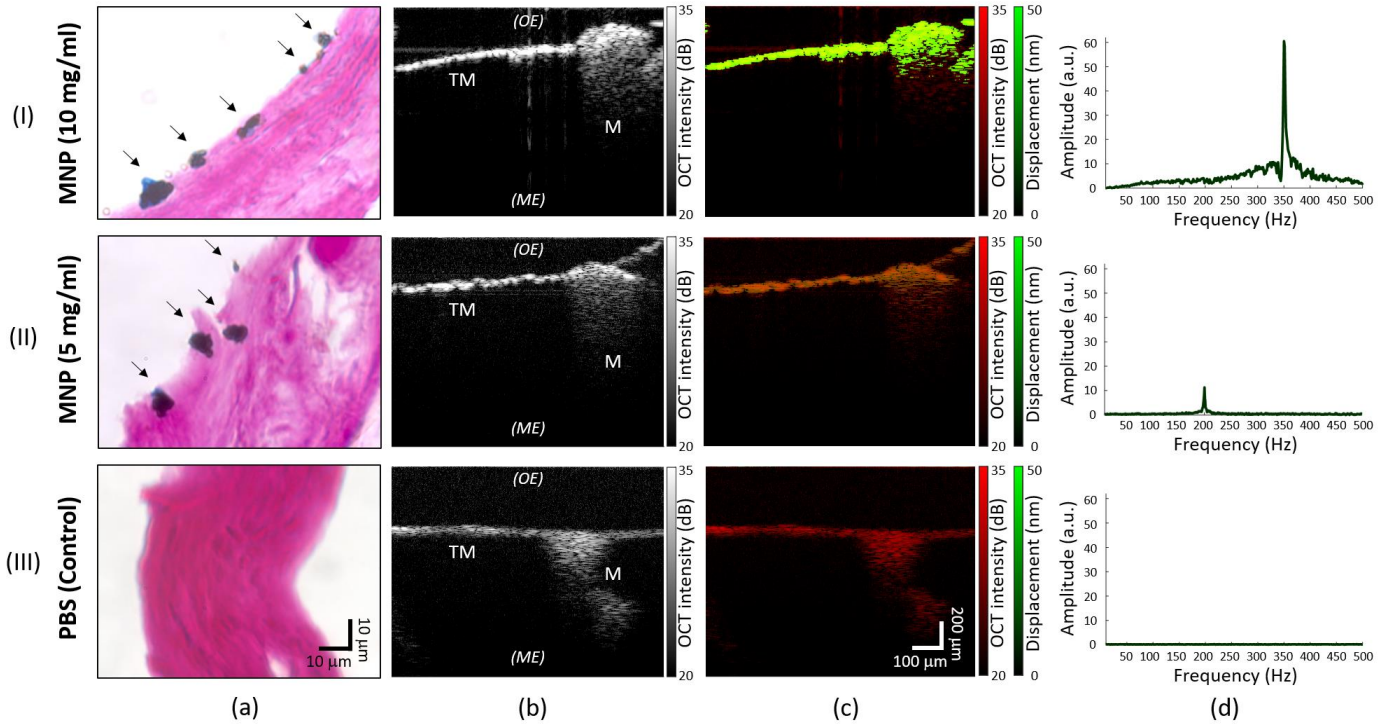

Fig. 4. Representative data of the TM samples applied with (I) 10 mg/ml MNP, (II) 5 mg/ml MNP, and (III) PBS solution (control). (a) Microscopic images (100x) of the representative histologic slices of TM tissues with iron-oxide staining. Indicated by the arrows, clusters of iron oxide MNPs (blue) are observed on the TM tissues (pink). (b) Representative structural OCT images and (c) the corresponding MM-OCT images of the TM samples that were mechanically perturbed around their resonance frequencies. In (c), structural intensity (red) is overlaid with the MM-displacement (green). (d) Frequency analysis of the three representative groups shows the existence of dominant frequencies in the mechanical spectra of the MNP-laden samples. Since the resonance frequency of each TM tissue sample is not the same, the dominant frequencies detected differ as well. Abbreviations: Outer ear (OE), middle ear (ME), and malleus (M).

This article has been accepted for publication in a future issue of this journal, but has not been fully edited. Content may change prior to final publication. Citation information: DOI 10.1109/TBME.2018.2819649, IEEE Transactions on Biomedical Engineering

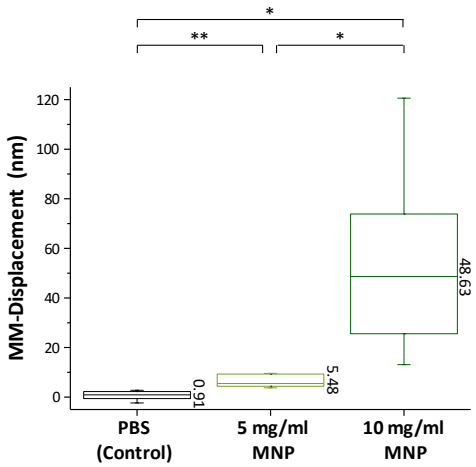

Fig. 5. Box plots of the MM-displacement amplitude of the rat TM samples applied with PBS (control), 5 mg/ml MNP, and 10 mg/ml MNP, where the total number of data points are N = 12, 12, 16, respectively. The median values of each group are indicated along the boxes. The symbols "*" and "**" denote *p*-values < 10^{-4} and 10^{-5}, respectively.

B. Magnetomotive Displacement Amplitude

To investigate the influence of the MNPs, the magnitudes of the MM-displacements were quantified and compared between the MNP-laden and the PBS-laden (control) TM tissues. Furthermore, the general influence of the MNP dosage applied to the TM was also explored. The MM-displacement amplitudes were evaluated on two groups of TM tissues applied with the same amount (0.1 ml) of MNP solution but at different concentrations – one lower (5 mg/ml) and the other higher (10 mg/ml). Note that as the MM-displacement amplitudes are frequency-dependent (detailed in C.), only the maximum displacement detected (at the resonant frequency) was included in the statistical pool for each individual TM sample.

Shown in Fig. 4 (c), larger MM-displacements were observed in the MNP-laden tissues as compared to those in the PBS-laden (control) tissues. Statistical analysis (Fig. 5) revealed a significant difference between the MNP-laden and the control group (*p*-value <10^{-4} between the 10 mg/ml MNP-laden and control groups; *p*-value <10^{-5} between the 5 mg/ml MNP-laden and control groups). This indicates that the application of MNP drops was necessary so that non-negligible magnetomotion could be generated. In the highly dosed group (10 mg/ml MNP), interestingly, the MM-displacement magnitudes induced on the *ex vivo* rat TM with the MM-setup were comparable to the acoustically-induced displacements excited with a sound pressure level (SPL) of 80–90 dB at 200–500 Hz excitation on cadaveric human TMs [23]. However, since rat TMs are stiffer than human TMs [50], a sound stimulation with even higher SPL may be needed in order to produce the same level of displacements on rat TMs.

A larger displacement was exhibited in the 10 mg/ml MNP-laden group (median 48.63 nm) as compared to that of the 5 mg/ml MNP-laden group (median 5.48 nm), while statistically significant differences were also observed (*p*-value <10^{-4}). Although this potentially manifests as a dependence on the MNP dosage, a comprehensive understanding of the correlation between the MNP dosage applied and the resulting MM-displacement amplitude should be further investigated by comparing more groups of MNP concentrations with an improved dosing control approach.

C. Spectroscopic Response of the TM

The human hearing capability varies with different auditory frequencies. To demonstrate the versatility of MM modulation and the capability for probing the responsive displacement of the MNP-laden TM tissue across various excitation frequencies

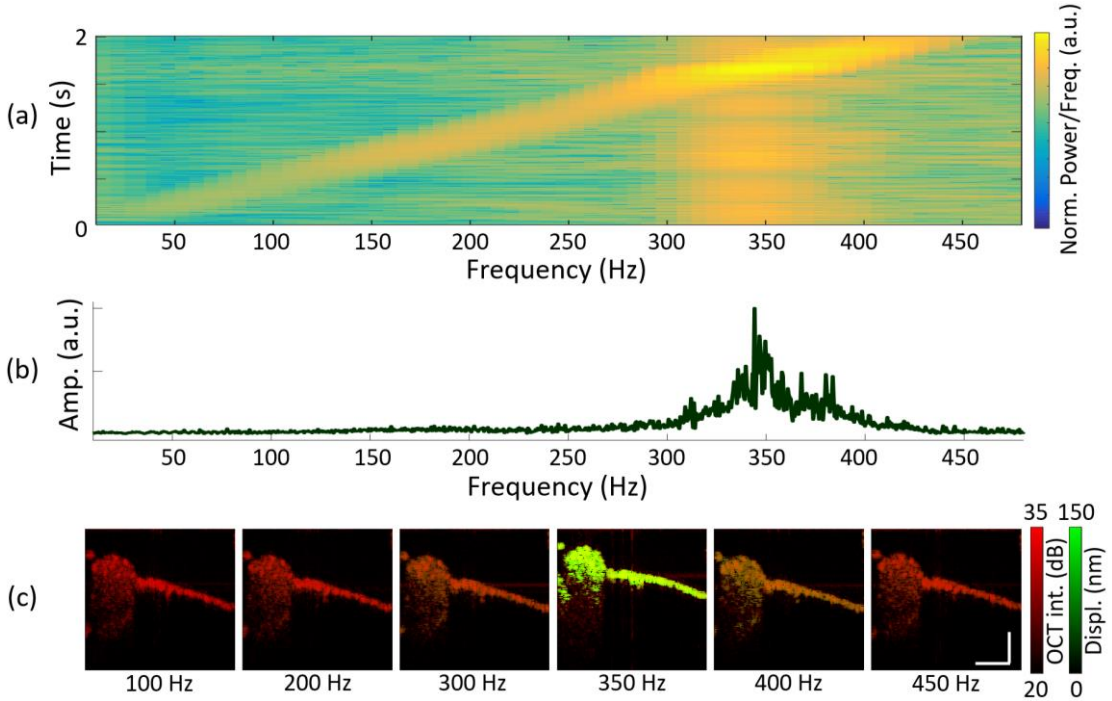

Fig. 6. Representative datasets showing the spectroscopic response of the MNP-laden TM tissue. After applying a chirped excitation (10–500 Hz) to the TM tissue, both (a) the spectrogram and (b) the mechanical spectrum showed that the largest mechanical vibration appeared around ~350 Hz. The spectroscopic response agrees with the trend shown in (c) the B-mode MM-OCT data, which show the superimposition of the structural image (red) and the spatial mapping of the MM-displacement (green) induced with various modulated frequencies. The scale bars represent ~200 μm.

This article has been accepted for publication in a future issue of this journal, but has not been fully edited. Content may change prior to final publication. Citation information: DOI 10.1109/TBME.2018.2819649, IEEE Transactions on Biomedical Engineering

at once, a chirped excitation was produced and the corresponding spectroscopic response was evaluated. The inherent nature of a chirped response is observed along the temporal axis of the spectrogram in Fig. 6 (a), where the dominant frequencies increase linearly with the increasing time points. From both the spectrogram and the mechanical spectrum (Fig. 6 (a, b)), higher amplitudes are observed at 300–400 Hz, while a mechanical amplitude peak is observed near 350 Hz. This agrees with the B-mode, oversampled MM-OCT datasets collected from the same tissue while a pure-tone harmonic oscillation was generated for each measurement. As shown in Fig. 6 (c), higher displacement is detected across the TM tissue when an excitation of 300, 350, and 400 Hz was given, and the induced TM movement reached its maximum at a modulated frequency of 350 Hz.

Although the assessment of the spectroscopic response was only demonstrated for *ex vivo* rat TM displacements here, this initial result implied the potential of using the MM setup to measure other frequency-dependent, hearing-aid-specific parameters on *in vivo* human ears in the future. Note that the *in vivo* spectroscopic response of the TM is expected to be quantitatively different from that of the excised specimens, as the non-intact middle ear cavity and the disrupted ossicular chain could result in a decreased resonant frequency and an increased displacement at lower frequencies (≤1 kHz) due to a reduced load from the cochlea and annular ligament on the TM [20-22, 51]. Interestingly, for non-intact TMs where only the malleus was attached, the resonant frequency observed from the rat here and that from the human [48] were in general agreement with one another, where a resonant frequency around 300–400 Hz could be observed in both cases.

D. Dynamics of Magnetomotive TM Motion

Finally, the spatiotemporal response of the MNP-laden TM tissue under a sinusoidal magnetic force was visualized by a vibration-amplified 4D-OCT dataset. Shown in Fig. 7 and Media 1, larger displacement magnitudes are seen at the malleus, and the closer the TM is to the malleus, the larger the movement. In addition, the frequency of the magnetomotion agrees with the modulated frequency (f_m = 460 Hz) of the magnetic force, as one cycle of movement is observed within ~2.2 ms. OCT has demonstrated its capability for 4D visualization of the MM-driven TM. Yet, a deeper understanding of the various contributing factors to the pattern of the TM motions is forseen in the future. For example, the fact that the strongest oscillation occurs at the malleus disagrees with previous observations [22, 23, 37], which could be a result of non-uniform distribution of MNPs (and hence magnetic force) on the TM. Additionally, it is hypothesized that the multiple minor oscillations that appear in Media 1 as the excitation force reached the maximum was a result of insufficient magnetic force strength provided at the non-resonance regime. These hypotheses can conceivably be validated in future OCT studies.

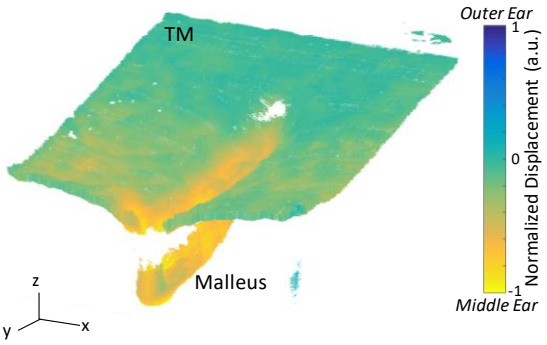

Fig. 7. Spatiotemporal visualization of the MM dynamics of an *ex vivo* rat TM tissue laden with MNPs. A sinusoidal magnetic force (460 Hz) was applied to the TM, where the representative frame shows the TM moving toward the middle ear directions. The corresponding vibration-amplified 4D-OCT dataset covering the TM motion of one entire sinusoidal cycle is provided in Media 1. The scale bars in each direction (x, y, and z) represent ~200 μm.

V. Discussion

Magnetomotive (MM) displacements and dynamics of *ex vivo* TMs containing MNPs have been demonstrated, using OCT for sensitive phase-resolved measurements. Based on this initial work, further investigations related to a MM-hearing aid configuration is needed before moving to *in vivo* animal and human studies. In terms of MNP delivery, the effect of diffusion time and magnetically-assisted diffusion schemes would need to be systematically explored. Although a permanent magnet may potentially assist the diffusion process [14], the strength of the static magnetic field and the time needed to allow for an effective guidance of the MNPs remains to be investigated. It is expected that the absence of the permanent magnet would result in a longer time needed for the MNPs to penetrate the TM and a less controllable MNP distribution. Additionally, non-invasive delivery of the MNPs deeper into the TM or the middle ear space can be conceivably implemented with advanced shaping of an external magnetic field. MM-displacements in the middle or inner ear can possibly be induced, and drugs could also be carried with the MNPs to allow for therapeutic purposes [15, 16, 59], while OCT imaging, with its capability of imaging the inner ear dynamics [60], can again serve as a visualization and/or validation tool. In addition, the spatial distribution of the MNPs across the TM can be systematically characterized by micro-CT [55], high-field MRI [56], and the emerging magnetic particle imaging (MPI) technique that detects the local concentration of ferromagnetic or superparamagnetic MNPs based on their nonlinear magnetization characteristics [61]. While MM-displacement has been successfully induced on the TM, it will also be interesting to investigate the movement of the ossicular chain in the middle ear that results from the induced MM-displacements. To increase the viability of the proposed MM scheme in hearing-aid-related applications, balancing between the position of the coil (e.g. in or outside of the ear canal) and the corresponding power requirement should also be carefully investigated. Although the efficacy of the magnetic field increases with shorter coil-to-TM distance [5, 6], undesirable acoustic feedbacks can be enhanced by the presence of coil in the ear canal.

A future *in vivo* study can potentially be conducted with the combined use of the MM-setup and a handheld, portable OCT system, which has previously enabled *in vivo* human ear imaging [31-33]. Additional hearing-aid associated parameters, such as the maximum equivalent pressure output (MEPO, the equivalent pressure needed to generate the same TM displacement induced from hearing device [5]), can potentially be measured with the help of a pneumatic-bulb-attached OCT probe and a pressure sensor [35]. While previous studies have suggested the benefit of using tissue-indwelling MNPs in otology [14, 19], it would be meaningful to directly examine the hypothesis that the minimal inertia of the MNPs could reduce the dampening effect of the TM, compared to the effect from a solid magnet transducer, in an *in vivo* study. With the readily available MM-setup, characterization of the biomechanical properties of the TM could be made possible by magnetomotive optical coherence elastography (MM-OCE) [12, 44, 47, 62].

Cytotoxicity and biosafety of the MNPs and the proposed MM-hearing aid scheme should be carefully considered for future clinical development. As a proof-of-concept study of the proposed MM-hearing scheme, bare metal MNPs were examined. However, a number of chemically-tailored MNPs have been reported to enable better colloidal stability, biocompatibility, and biodegradability, which are forseen to be incorporated. For instance, undesirable iron exposure and production of free radicals can be prevented by using silica-coated MNPs [14, 19]. In addition, enhanced miscibility in aqueous solution can be achieved by coating the MNP with polymers such as dextran and polyethylene glycol (PEG) [63]. In fact, successful cellular uptake of the silica-coated MNPs in the middle ear epithelial tissue and delivery of the polymer-coated MNPs to the round window membrane in the inner ear have been reported previously [14, 58]. Biosafety concerns imposed by the magnetic parameters (e.g. frequency and field strength) of the MM setup should be investigated as well. The low frequencies applied here (10–500 Hz) will not induce ionization [64]. Compared to the transceiving band of cochlear implants (MHz regime) and wireless hearing aids (GHz regime), the low frequency of the MM setup can better avoid radiofrequency (RF)-induced thermal injury. Additionally, the driving voltage for the external coil used here (8V peak) is slightly larger than, yet of the same order of magnitude as, the maximum allowable voltage to be induced on the implanted receiver coil in a cochlea implant (6V peak) [65]. In comparison to the dynamic magnetic field used in other clinical techniques, our AMF frequency range was higher than that of transcranial magnetic stimulation (TMS) (<20 Hz) but lower than that of MRI (RF 10–400 MHz). Additionally, the magnetic field strength applied here (<0.02 T at 2 mm) was orders of magnitude lower than that of TMS (1.5–3 T) [66]. Therefore, it is hypothesized that the proposed MM scheme can meet the biosafety requirements for the human body, which should be carefully examined in the future.

Sound-induced motions on TMs are well-known to be frequency-dependent and inherently complex, while standing-wave-like modal motions and/or traveling-wave-like motions were observed on TM surfaces previously [22, 23, 37] and numerous hypotheses and models of the TM motion mechanisms have been actively investigated for at least 5 decades [23]. In this preliminary study, generally in-phase motions were observed via OCT imaging, which agrees with the trend of the surface motions of the *ex vivo* TM stimulated with a low-frequency sound source (≤1 kHz). However, complex TM vibration patterns showing spatial maxima and minima moving out of phase with one another have been reported on TM samples stimulated with higher frequencies [22, 23, 37]. Before the development of a clinical device, it would be important to compare the dynamics of the MNP-laden TM with those induced with different frequencies from the same specimen and investigate the potential hearing effects caused by different vibration patterns. Moreover, the performance of the proposed MM-hearing scheme can be compared with conventional acoustic hearing aids by characterizing the frequency-dependent modal vibrations of the MNP-laden TMs under various AMF strengths and quantifying the motions exhibited on the TM stimulated by ambient sound sources (e.g. by a speaker) with various frequencies and SPLs.

VI. Conclusion

Magnetomotive displacements of MNP-laden TM tissues have been successfully demonstrated using the proposed setup, along with the evaluation and quantification of the magnetomotion by phase-sensitive OCT. The evidence of effective MNP diffusion into the *ex vivo* rat TM tissues was revealed by Prussian blue iron-oxide staining of histological sections of the TM tissues. Results demonstrated that significantly larger displacement magnitudes were observed only from the MNP-laden tissues, suggesting a direct influence of the MNPs in generating and modulating the magnetomotion of the TM tissues. In addition, other than a pure-tone excitation, the capability of generating a chirped excitation and detecting the spectroscopic response was also demonstrated. Finally, spatiotemporal visualization of the TM vibration was enabled by the acquisition of a 4D-OCT dataset.

In conclusion, this paper demonstrates the feasibility of using the magnetomotive principle and technology to directly induce vibrations on MNP-laden TM tissues, which could potentially enhance sound perception. In the future, an integrated system combining the receiver, processor, magnetic coil, and MNP transducers are envisioned. Ambient sounds can be detected, processed, converted to electric signals to drive the magnetic coil, and subsequently produce modulated AMF so that vibrations can be induced on the MNP-laden TM accordingly. Afterward, the artificially generated acoustic waves can be transferred from the TM to the inner ear. Since the modulated movement can be generated without any auditory speech sources from the outer ear, it may be possible to allow one to "hear without ambient sounds". For instance, a modulated and targeted radio wave input signal can be detected and directly transferred from the receiver to the magnetic coil, which may potentially enable speech-free military or surveillance applications in the future.

Acknowledgment

This project was supported in part by grants from the National Institutes of Health (R01 EB013723 and R01 CA213149). We would like to thank Dr. Kush Paul for his assistance with some of the initial animal handling in this study.

Additional information can be found at: http://biophotonics.illinois.edu.

REFERENCES

[1] B. Yueh *et al.*, "Screening and management of adult hearing loss in primary care: Scientific review," *JAMA,* vol. 289, no. 15, pp. 1976-1985, 2003.

[2] F. R. Lin *et al.*, "Hearing loss prevalence in the United States," *Arch. Intern. Med.,* vol. 171, no. 20, pp. 1851-1853, 2011.

[3] G. Sprinzl, and H. Riechelmann, "Current trends in treating hearing loss in elderly people: A review of the technology and treatment options–A mini-review," *Gerontology,* vol. 56, no. 3, pp. 351-358, 2010.

[4] T. Moser *et al.*, "Review of hair cell synapse defects in sensorineural hearing impairment," *Otol. Neurotol.,* vol. 34, no. 6, pp. 995-1004, 2013.

[5] R. Perkins *et al.*, "The EarLens system: New sound transduction methods," *Hear. Res.,* vol. 263, no. 1, pp. 104-113, 2010.

[6] R. Perkins, "Earlens∗ tympanic contact transducer: A new method of sound transduction to the human ear," *Otolaryngol. Head Neck Surg.,* vol. 114, no. 6, pp. 720-728, 1996.

[7] J. R. Tysome *et al.*, "Systematic review of middle ear implants: do they improve hearing as much as conventional hearing aids?," *Otol. Neurotol.,* vol. 31, no. 9, pp. 1369-1375, 2010.

[8] S. Reinfeldt *et al.*, "New developments in bone-conduction hearing implants: A review," *Med. Devices (Auckl.),* vol. 8, pp. 79, 2015.

[9] J. B. Hunter *et al.*, "The ototronix MAXUM middle ear implant for severe high-frequency sensorineural hearing loss: Preliminary results," *Laryngoscope,* vol. 126, no. 9, pp. 2124-2127, 2016.

[10] J. P. Fay *et al.*, "Preliminary evaluation of a light based contact hearing device for the hearing impaired," *Otol. Neurotol.,* vol. 34, no. 5, pp. 912, 2013.

[11] C.-F. Lee *et al.*, "A novel opto-electromagnetic actuator coupled to the tympanic membrane," *J. Biomech.,* vol. 41, no. 16, pp. 3515-3518, 2008.

[12] P.-C. Huang *et al.*, "Magnetomotive optical coherence elastography for magnetic hyperthermia dosimetry based on dynamic tissue biomechanics," *IEEE J. Sel. Top. Quantum Electron.,* vol. 22, no. 4, pp. 1-16, 2016.

[13] A. Hu, and L. S. Parnes, "Intratympanic steroids for inner ear disorders: A review," *Audiol. Neurotol.,* vol. 14, no. 6, pp. 373-382, 2009.

[14] K. Dormer *et al.*, "Epithelial internalization of superparamagnetic nanoparticles and response to external magnetic field," *Biomaterials,* vol. 26, no. 14, pp. 2061-2072, 2005.

[15] B. Shapiro *et al.*, "Shaping magnetic fields to direct therapy to ears and eyes," *Annu. Rev. Biomed. Eng.,* vol. 16, pp. 455-481, 2014.

[16] D. A. Depireux *et al.*, "Magnetic delivery of therapy to the cochlea," *Hear. J.,* vol. 70, no. 7, pp. 14-16, 2017.

[17] H. Arami *et al.*, "*In vivo* delivery, pharmacokinetics, biodistribution and toxicity of iron oxide nanoparticles," *Chem. Soc. Rev.,* vol. 44, no. 23, pp. 8576-8607, 2015.

[18] S. Laurent *et al.*, "Magnetic iron oxide nanoparticles: synthesis, stabilization, vectorization, physicochemical characterizations, and biological applications," *Chem. Rev.,* vol. 108, no. 6, pp. 2064-110, 2008.

[19] R. D. Kopke *et al.*, "Magnetic nanoparticles: inner ear targeted molecule delivery and middle ear implant," *Audiol. Neurotol.,* vol. 11, no. 2, pp. 123-133, 2006.

[20] A. M. Huber *et al.*, "Evaluation of eardrum laser Doppler interferometry as a diagnostic tool," *Laryngoscope,* vol. 111, no. 3, pp. 501-507, 2001.

[21] J. J. Rosowski *et al.*, "Clinical utility of laser-Doppler vibrometer measurements in live normal and pathologic human ears," *Ear Hear.,* vol. 29, no. 1, pp. 3, 2008.

[22] H. Wada *et al.*, "Vibration measurement of the tympanic membrane of guinea pig temporal bones using time-averaged speckle pattern interferometry," *J. Acoust. Soc. Am.,* vol. 111, no. 5, pp. 2189-2199, 2002.

[23] J. T. Cheng *et al.*, "Wave motion on the surface of the human tympanic membrane: holographic measurement and modeling analysis," *J. Acoust. Soc. Am.,* vol. 133, no. 2, pp. 918-937, 2013.

[24] D. Huang *et al.*, "Optical coherence tomography," *Science,* vol. 254, no. 5035, pp. 1178-1181, 1991.

[25] M. R. Hee *et al.*, "Optical coherence tomography of the human retina," *Arch. Ophthalmol.,* vol. 113, no. 3, pp. 325-332, 1995.

[26] W. Drexler, and J. G. Fujimoto, "State-of-the-art retinal optical coherence tomography," *Prog. Retin. Eye Res.,* vol. 27, no. 1, pp. 45-88, 2008.

[27] S. J. Erickson-Bhatt *et al.*, "Real-time imaging of the resection bed using a handheld probe to reduce incidence of microscopic positive margins in cancer surgery," *Cancer Res.,* vol. 75, no. 18, pp. 3706-3712, 2015.

[28] F. T. Nguyen *et al.*, "Intraoperative evaluation of breast tumor margins with optical coherence tomography," *Cancer Res.,* vol. 69, no. 22, pp. 8790-8796, 2009.

[29] M. Mogensen *et al.*, "Optical coherence tomography for imaging of skin and skin diseases." pp. 196-202.

[30] P.-C. Huang *et al.*, "Quantitative characterization of mechanically indented *in vivo* human skin in adults and infants using optical coherence tomography," *J. Biomed. Opt.,* vol. 22, no. 3, pp. 034001-034001, 2017.

[31] C. T. Nguyen *et al.*, "Noninvasive *in vivo* optical detection of biofilm in the human middle ear," *Proc. Natl. Acad. Sci. U.S.A.,* vol. 109, no. 24, pp. 9529-9534, 2012.

[32] C. T. Nguyen *et al.*, "Investigation of bacterial biofilm in the human middle ear using optical coherence tomography and acoustic measurements," *Hear. Res.,* vol. 301, pp. 193-200, 2013.

[33] G. L. Monroy *et al.*, "Noninvasive depth-resolved optical measurements of the tympanic membrane and middle ear for differentiating otitis media," *Laryngoscope,* vol. 125, no. 8, 2015.

[34] C. T. Nguyen *et al.*, "Non-invasive optical interferometry for the assessment of biofilm growth in the middle ear," *Biomed. Opt. Express,* vol. 1, no. 4, pp. 1104-1116, 2010.

[35] R. L. Shelton *et al.*, "Quantitative pneumatic otoscopy using a light-based ranging technique," *J. Assoc. Res. Otolaryngol.,* 2017.

[36] H. M. Subhash *et al.*, "Feasibility of spectral-domain phase-sensitive optical coherence tomography for middle ear vibrometry," *J. Biomed. Opt.,* vol. 17, no. 6, pp. 0605051-0605053, 2012.

[37] E. W. Chang *et al.*, "Simultaneous 3D imaging of sound-induced motions of the tympanic membrane and middle ear ossicles," *Hear. Res.,* vol. 304, pp. 49-56, 2013.

[38] D. MacDougall *et al.*, "Long-range, wide-field swept-source optical coherence tomography with GPU accelerated digital lock-in Doppler vibrography for real-time, *in vivo* middle ear diagnostics," *Biomed. Opt. Express,* vol. 7, no. 11, pp. 4621-4635, 2016.

[39] J. Park *et al.*, "Investigation of middle ear anatomy and function with combined video otoscopy-phase sensitive OCT," *Biomed. Opt. Express,* vol. 7, no. 2, pp. 238-250, 2016.

[40] A. L. Oldenburg *et al.*, "Imaging magnetically labeled cells with magnetomotive optical coherence tomography," *Opt. Lett.,* vol. 30, no. 7, pp. 747-9, 2005.

[41] A. L. Oldenburg *et al.*, "Magnetomotive contrast for *in vivo* optical coherence tomography," *Opt. Express,* vol. 13, no. 17, pp. 6597-614, 2005.

[42] A. L. Oldenburg *et al.*, "Phase-resolved magnetomotive OCT for imaging nanomolar concentrations of magnetic nanoparticles in tissues," *Opt. Express,* vol. 16, no. 15, pp. 11525-39, 2008.

[43] R. John *et al.*, "*In vivo* magnetomotive optical molecular imaging using targeted magnetic nanoprobes," *Proc. Natl. Acad. Sci. U.S.A.,* vol. 107, no. 18, pp. 8085-8090, 2010.

[44] A. L. Oldenburg *et al.*, "Imaging and elastometry of blood clots using magnetomotive optical coherence tomography and labeled platelets," *IEEE J. Sel. Top. Quantum Electron.,* vol. 18, no. 3, pp. 1100-1109, 2012.

[45] S. A. Boppart *et al.*, "Optical probes and techniques for molecular contrast enhancement in coherence imaging," *J. Biomed. Opt.,* vol. 10, no. 4, pp. 41208, 2005.

[46] S. S. Shevkoplyas *et al.*, "The force acting on a superparamagnetic bead due to an applied magnetic field," *Lab Chip,* vol. 7, no. 10, pp. 1294-1302, 2007.

[47] V. Crecea *et al.*, "Magnetomotive nanoparticle transducers for optical rheology of viscoelastic materials," *Opt. Express,* vol. 17, no. 25, pp. 23114-22, 2009.

[48] D. De Greef *et al.*, "Viscoelastic properties of the human tympanic membrane studied with stroboscopic holography and finite element modeling," *Hear. Res.,* vol. 312, pp. 69-80, 2014.

[49] A. Ahmad *et al.*, "Magnetomotive optical coherence elastography using magnetic particles to induce mechanical waves," *Biomed. Opt. Express*, vol. 5, no. 7, pp. 2349-2361, 2014.

[50] J. J. Rosowski, "Outer and middle ears," *Comparative Hearing: Mammals*, R. R. Fay and A. N. Popper, eds., pp. 172-247, New York, NY: Springer New York, 1994.

[51] M. Vlaming, and L. Feenstra, "Studies on the mechanics of the normal human middle ear," *Clin. Otolaryngol.*, vol. 11, no. 5, pp. 353-363, 1986.

[52] S. Van der Jeught *et al.*, "Full-field thickness distribution of human tympanic membrane obtained with optical coherence tomography," *J. Assoc. Res. Otolaryngol.*, vol. 14, no. 4, pp. 483-494, 2013.

[53] H. Abdi, "Holm's sequential Bonferroni procedure," *Encyclopedia of Research Design*, 8, 2010.

[54] D. Zanella *et al.*, "Iron oxide nanoparticles can cross plasma membranes," *Sci. Rep.*, vol. 7, no. 1, pp. 11413, 2017.

[55] Y. Torrente *et al.*, "High-resolution X-ray microtomography for three-dimensional visualization of human stem cell muscle homing," *FEBS Lett.*, vol. 580, no. 24, pp. 5759-5764, 2006.

[56] E. M. Shapiro *et al.*, "Sizing it up: Cellular MRI using micron-sized iron oxide particles," *Magn. Reson. Med.*, vol. 53, no. 2, pp. 329-338, 2005.

[57] X. Khoo *et al.*, "Formulations for trans-tympanic antibiotic delivery," *Biomaterials*, vol. 34, no. 4, pp. 1281-1288, 2013.

[58] X. Du *et al.*, "Magnetic targeted delivery of dexamethasone acetate across the round window membrane in guinea pigs," *Otol. Neurotol.*, vol. 34, no. 1, pp. 41, 2013.

[59] J.-H. Lee *et al.*, "Magnetic nanoparticles for ultrafast mechanical control of inner ear hair cells," *ACS Nano*, vol. 8, no. 7, pp. 6590-6598, 2014.

[60] H. Y. Lee *et al.*, "Noninvasive *in vivo* imaging reveals differences between tectorial membrane and basilar membrane traveling waves in the mouse cochlea," *Proc. Natl. Acad. Sci. U.S.A.*, vol. 112, no. 10, pp. 3128-3133, 2015.

[61] J. Borgert *et al.*, "Magnetic particle imaging," *Springer Handbook of Medical Technology*, R. Kramme, K.-P. Hoffmann and R. S. Pozos, eds., pp. 461-476, Berlin, Heidelberg: Springer Berlin Heidelberg, 2011.

[62] A. Ahmad *et al.*, "Mechanical contrast in spectroscopic magnetomotive optical coherence elastography," *Phys. Med. Biol.*, vol. 60, no. 17, pp. 6655-68, 2015.

[63] C. Boyer *et al.*, "The design and utility of polymer-stabilized iron-oxide nanoparticles for nanomedicine applications," *NPG Asia Mater.*, vol. 2, no. 1, pp. 23-30, 2010.

[64] V. Hartwig *et al.*, "Biological effects and safety in magnetic resonance imaging: a review," *Int. J. Environ. Res. Public Health*, vol. 6, no. 6, pp. 1778-1798, 2009.

[65] C. Teissl *et al.*, "Magnetic resonance imaging and cochlear implants: Compatibility and safety aspects," *J. Magn. Reson. Imaging.*, vol. 9, no. 1, pp. 26-38, 1999.

[66] P. G. Janicak, and M. E. Dokucu, "Transcranial magnetic stimulation for the treatment of major depression," *Neuropsychiatr. Dis. Treat.*, vol. 11, pp. 1549, 2015.